

Diffusion of hydrogen in bcc tungsten studied with first principle calculations

K. Heinola^{a)} and T. Ahlgren

Accelerator Laboratory, University of Helsinki, P.O. Box 43, FIN-00014 Helsinki, Finland

(Received 5 October 2009; accepted 11 March 2010; published online 9 June 2010)

First principle calculations were used to study the hydrogen migration properties in bulk bcc tungsten. Hydrogen has low solubility in tungsten and occupies the tetrahedral interstitial site with an energy difference of 0.38 eV compared to the octahedral interstitial site. The hydrogen diffusion coefficient was evaluated using the harmonic transition state theory and was found to agree with the experimental results at temperatures above 1500 K. The height of the migration barrier between two adjacent tetrahedral sites was found to be 0.21 eV, which is lower than the value 0.39 eV obtained for the migration barrier from degassing measurements in the temperature range between 1100 and 2400 K. The tunneling correction to the diffusion rate provides much better agreement with the experimental result at 29 K than the extrapolated experimental D from high temperature measurements. © 2010 American Institute of Physics. [doi:10.1063/1.3386515]

I. INTRODUCTION

Tungsten (W) is used in a large number of industrial applications due to its special mechanical and thermal properties. These extraordinary properties¹ have validated W to be used as divertor plate material in the next step fusion device ITER, where the divertor region will be subjected to high heat and particle flux from the plasma.² Low-energy (1–100 eV) H isotopes escaping the plasma and high-temperature He as a byproduct from the fusion reaction, can congregate on the W surface or when having high energies or high fluxes, penetrate through it and diffuse deeper into the bulk. These solute light elements have low solid solubility but high mobility in W.

Hydrogen isotopes and He can be easily immobilized by other impurity atoms present in the lattice, on the surfaces of the grain boundaries, at dislocations and voids, or by other lattice imperfections that can act as active trapping sites. However, an important difference between He and H in W is the self-trapping of He to another He at a solute site shown by several experimental studies and density functional theory (DFT) calculations,³ whereas H does not get self-trapped according to jellium model calculations⁴ and recent DFT calculations.^{5,6}

The accumulation of H and He into these snares can lead to modification of the material's mechanical and physical properties. H and He build-up in cavities, voids, and platelets can enhance bubble growth and blistering in the material. Moreover, in the case of H, the picture of blister mechanism is somewhat unclear since the measured thicknesses of the blister covers are orders of magnitude larger than the projected range of H ions.⁷ He blisters are formed at the depth of the projected range.

Many experimental and computational analyses on recycling and retention of H in W need the diffusion velocity and energetics information as input. Therefore, the study of the

interstitial diffusivity of hydrogen in W is vital, albeit difficult because the effect of trapping becomes a rate limiting step unless the operating temperature is above the trapping energies or the concentration of traps is negligible. Experimental work on hydrogen diffusivity above room temperature (RT) has been carried out by Moore and Unterwald⁸ (1200 K < T < 2500 K), Ryabchikov⁹ (1900 K < T < 2400 K), Frauenfelder¹⁰ (1100 K < T < 2400 K), Zakharov *et al.*¹¹ (910 K < T < 1060 K), and Benamati *et al.*¹² (850 K < T < 885 K). All these studies are based on degassing and permeation experiments, that are indirect measurements of hydrogen concentrations. The widely used and recommended¹³ reference value for H diffusion in tungsten is $D = 4.1 \times 10^{-7} \exp(-0.39 \text{ eV}/kT) \text{ m}^2/\text{s}$ obtained by Frauenfelder.¹⁰ In that work the temperatures used are so high that trapping phenomena can be expected to be unimportant. Furthermore, the temperature range covered by the measurements is wide enough to determine activation energy and pre-exponential factor with a low statistical error. An additional merit of that work is that the samples were carefully hydrogenated in order to produce the H concentration that was assumed to be constant throughout the samples according to Sievert's law. The earlier investigations at high temperatures by Moore and Ryabchikov provided deviating results ($D = 7.25 \times 10^{-8} \exp(-1.80 \text{ eV}/kT) \text{ m}^2/\text{s}$ and $D = 8.1 \times 10^{-6} \exp(-0.86 \text{ eV}/kT) \text{ m}^2/\text{s}$, respectively) since the H concentrations presumably had strong deviations from a uniform constant concentration which was presupposed in their calculations. Reported experimental diffusivities at temperatures above RT but under 1100 K are strongly limited by trapping mechanisms since the diffusivities fall clearly under the extrapolated result by Frauenfelder at these temperatures. Moreover, it has been suggested by Serra *et al.*¹⁴ and Benamati *et al.*¹² that trapping phenomenon influence the hydrogen diffusion at temperatures under 1473 K.

Direct measurements of hydrogen concentrations for diffusion studies in W has been done at temperatures less than 100 K by Macrander and Seidman,¹⁵ who measured H con-

^{a)}Electronic mail: kalle.heinola@helsinki.fi.

concentrations at 29 K and by Panitz,¹⁶ who measured the deuterium profiles at 80 K. In those experiments the W samples were thought to be defect free, perfect crystals without *a priori* and implantation induced defects. This was concluded based on the pretreatment of the samples and the fact that the hydrogen concentrations were produced with implantation energies that yield to collision energies far below the minimum displacement energy (~ 42 eV) (Ref. 17) for a stable Frenkel pair in W. At such low temperatures, hydrogen is classically immobile at an interstitial site. However, from the fact that the extrapolated diffusivity by Frauenfelder at 29 K is $\sim 10^{52}$ times lower than the diffusivity by Macrander and Seidman $D(29\text{ K}) = (1-10) \times 10^{-22}$ m²/s, it is evident that H and its isotopes must be treated nonclassically at low temperatures.

The aim of this work is to study for the first time the diffusivity of H in W using the first principle method. The transition state theory (TST) is employed for describing the quantum mechanical effects of hydrogen diffusion and the tunneling correction for the hydrogen hopping rate has been taken into account.

Calculations based on electron DFTs can be considered as state of the art theoretical research method in the fields of material physics and chemistry. DFTs are based only on the knowledge of the electronic structure of the material's elementary atoms and are therefore recurrently called as *ab initio* method since any other information of the material is not needed. As a result, all the physical and chemical properties of the system can be concluded up to certain extent. DFT calculations have their limitations due to the restricted validity of the functionals used and because the number of atoms that can be considered in a study is bounded by the computational power available. In a modern computing cluster environment, systems up to hundreds of atoms can be examined. Since even these are only microscopical systems compared to average experimental entities ($\sim 10^{22}$ atoms/cm³), the DFT results must undergo careful criticism when extrapolated into larger realistic dimensions. On the other hand, DFT calculations can give insight and detailed information about systems which are not experimentally approachable directly.

The outline of this paper is as follows. In Sec. II A the computational details are presented. Sec. II B demonstrates the theoretical background for calculating the jump rate and diffusion constant. The results from bulk W calculations will be presented in Secs. III A and III B covers the H diffusion in W. Sec. III C is focused on the effect of tunneling and on the isotope effect on the jump rate.

II. COMPUTATIONAL METHOD AND THEORETICAL BACKGROUND

A. Calculations

The DFT calculations for energetics of hydrogen and tungsten systems were done with the VIENNA AB INITIO SIMULATION PACKAGE (VASP).¹⁸⁻²⁰ The electronic groundstate of the system was calculated using the projector-augmented wave^{21,22} potentials as provided in VASP. The electron exchange-correlation was described within the generalized

gradient approximation using Perdew–Burke–Ernzerhof (PBE) (Refs. 23 and 24) functionals. The charge density was represented on a real space grid of 0.035 Å. The six outermost electrons of the W atom were used as valence electrons (d^5s^1 configuration). The spin unpolarized electrons were given an artificial temperature $\sigma=0.15$ eV and the partial occupancies were integrated with the Methfessel and Paxton method²⁵ of the first order in order to keep the difference of free and total energy less than 1 meV/atom in all calculations. In order to determine the energies, their values obtained at finite artificial temperature were extrapolated to a vanishing artificial temperature.

For the volumetric and ionic relaxation the conjugate gradient algorithm²⁶ was used and the relaxation was stopped after a convergence criterion of 0.01 eV/Å was reached. The energy cutoff for calculations was 450 eV which ensured the convergence of geometrical structures and total energies. A $3 \times 3 \times 3$ k-point mesh was sampled by the Monkhorst and Pack scheme.²⁷ A $4 \times 4 \times 4$ super cell was used for body-centered cubic (bcc) tungsten with 128 atoms. Using periodic boundary conditions for the simulation cell and with one H atom on the interstitial site an impurity concentration less than 1% was obtained. The lattice distortion around an H atom is small compared to the cell size used and has negligible displacement effect on the outermost W atoms in the cell. To validate the parameters used in the current DFT study, we performed comparative calculations for different phases of bulk tungsten and for H solution in the bulk phase. These results and the results from the dimer configuration calculations, were then compared with the experimental results and other DFT calculations found in the literature. The migration barrier for hydrogen diffusion was calculated using the nudged elastic band (NEB) method.^{28,29} The calculation parameters and convergence criteria were kept the same as in the ground state calculations.

B. Diffusion of light interstitials

The diffusion rate of atomic interstitials in solid solutions is generally expressed as $D = D_0 \times e^{-E_m/kT}$, where D_0 is usually the temperature independent pre-exponential factor, T temperature, and k Boltzmann constant. E_m is the minimum height of the potential barrier, which the diffusing particle must overcome from an equilibrium site to advance along the diffusion path to another equilibrium site. According to the diffusion theory presented by Wert and Zener,³⁰⁻³² the diffusion rate can be written as $D = \gamma a^2 \Gamma$, where γ is the geometrical factor and a the lattice parameter of the host lattice. $\Gamma = \nu_0 \times e^{-E_m/kT}$ is the jump rate at which the interstitial jumps to the nearest equilibrium site and ν_0 is the frequency of vibration of a solute atom in an interstitial position. For the tetrahedral interstitial diffusion in bcc lattice the geometrical factor $\gamma = 1/48$ and the jump length $\lambda = a/\sqrt{8}$, yield

$$D = \frac{1}{6} \lambda^2 \Gamma. \quad (1)$$

The form of Eq. (1) holds for interstitial and substitutional diffusion in primitive cubic lattices, i.e., simple cubic, face-centered cubic (fcc), and bcc lattice.³³

The jump rate Γ has been calculated in this work with the concept of activated complex for reaction rates by Eyring^{34,35} within the transition state method by Wigner.^{36,37} This statistical approach constitutes the well-known TST. The basic assumptions in TST is as follows: (a) the motion of the nuclei can be described by classical mechanics, (b) the rapidly moving electrons are in their lowest quantum state and follow the comparably slowly moving nuclei at every position, and (c) all reactants reaching the transition state, i.e., activated point for chemical reactions and saddle point for diffusion process, will advance along the reaction coordinate. The general expression for the reaction rate, i.e., the jump rate for diffusion is expressed in TST as $\Gamma = (Z_a/Z)v = (Z_a/Z)(p/m^*)$, where Z_a and Z are the total partition functions of the activated state and the ground state, respectively, multiplied by the reactant's average velocity $v = (p/m^*)$ per unit length on the activated state.³⁴ Integrating over $p = 0 \dots \infty$ yields

$$\Gamma = \frac{kT}{h} \times \frac{Z'_a}{Z} e^{-\Delta E/kT}, \quad (2)$$

where Z'_a is the partition function of the activated state for all the other normal coordinates except in the direction of the reaction coordinate. The term $(kT/h)e^{-\Delta E/kT}$ includes the translational partition function in this coordinate. ΔE is the energy difference of the activated point and ground state and corresponds to the migration barrier E_m . Equation (2) can be solved for the diffusion jump rate using either classical or quantum mechanical solution for the vibrational partition function. Studying purely diffusion, without any chemical reactions at the activated point, the partition functions for the momentum of inertia at the saddle point and ground state cancel out in Eq. (2). The small vibrations at both states are taken to be harmonic oscillations. Using the classical solution of the vibrational partition function yields

$$\Gamma_{cl} = \frac{\prod_i^{3N} \nu_i}{\prod_i^{3N-1} \nu_i^{\ddagger}} e^{-\Delta E/kT}, \quad (3)$$

where ν_i and ν_i^{\ddagger} are the real normal modes of vibration on the ground state and activation state, respectively. N is the number of the vibrating atoms. Equation (3) is the result of Vineyard.³⁸ Noteworthy is that the potential energy has negative curvature along the reaction coordinate at the saddle point yielding an imaginary vibration mode, ν^* . Thus, there is one real normal mode less at the saddle point than at the ground state. Using the quantum mechanical solution of the vibrational partition function, the jump rate can be presented as

$$\Gamma_{\text{hTST}} = \frac{kT}{h} \times \frac{\prod_i^{3N-1} \left(\frac{e^{-h\nu_i^{\ddagger}/2kT}}{1 - e^{-h\nu_i^{\ddagger}/kT}} \right)}{\prod_i^{3N} \left(\frac{e^{-h\nu_i/2kT}}{1 - e^{-h\nu_i/kT}} \right)} e^{-\Delta E/kT}. \quad (4)$$

Equation (4) is the harmonic TST (hTST) jump rate. At high temperatures ($kT \gg h\nu$) the result of Vineyard is obtained. In the low temperature region ($kT \ll h\nu$) the Eq. (4) yields

$$\begin{aligned} \Gamma_{\text{hTST}} &= \frac{kT}{h} \times \frac{\prod_i^{3N} (1 - e^{-h\nu_i/kT})}{\prod_i^{3N-1} (1 - e^{-h\nu_i^{\ddagger}/kT})} \\ &\times \exp \left[\left(-\Delta E - \sum_i^{3N-1} \frac{h\nu_i^{\ddagger}}{2} + \sum_i^{3N} \frac{h\nu_i}{2} \right) \times \frac{1}{kT} \right] \\ &\approx \frac{kT}{h} \exp \left[-(\Delta E + \Delta E_{\text{ZPE}}) \times \frac{1}{kT} \right]. \end{aligned} \quad (5)$$

From the quantum mechanical solution of the jump rate, Eq. (4), two conclusions are apparent, (1) the jump rate has a temperature dependent pre-exponential factor, which does not exist in the classical solution and (2) the difference in the vibrational energies of the saddle point and the ground state, i.e., the zero-point correction ($\Delta E_{\text{ZPE}} = \sum 1/2h\nu^{\ddagger} - \sum 1/2h\nu$), influences the energy needed for a particle to jump over the migration barrier. Determining the jump rate in TST one has to calculate only the potential barrier and the vibrational properties at the potential minimum and at the saddle point.

In this work, the hydrogen jump rate was deduced from the DFT phonon calculations at the ground state and at the activated point. The Hessian matrix was determined using finite differences, i.e., by displacing the vibrating atom in the direction of each cartesian coordinate and calculating the second derivative of the energy. Since hydrogen is a light mass particle and therefore has a high vibrational energy at zero point, the quantum mechanical vibration effects are included. Hence Eq. (4) was used for the hydrogen jump rate calculations between RT and 2500 K.

The number of applications utilizing the combination of DFT and TST is increasing. Self-diffusion calculations in Al (Refs. 39 and 40) have shown, that the migration frequencies calculated within the harmonic TST gives diffusion coefficients which are in agreement with the experimental data which span over a region of ten orders of magnitude. For the H studies, consistency with experimental results have been obtained for the rates of H in Nb and Ta using Eq. (5).⁴¹ For H in bcc Fe (Ref. 42) using TST, the computational diffusion constant was found within the experimental values. DFT studies using the TST jump rate on diffusion of H on Cu (001) surface have been found to be in good agreement with the experimental results.⁴³ In all the above mentioned H studies, TST have been used for calculating the jump rate at temperatures where the tunneling effect is negligible. At temperatures below certain crossover, tunneling effect of H becomes dominant and cannot be neglected. The tunneling will be discussed in Sec. III C.

III. RESULTS AND DISCUSSION

A. Tungsten

Extensive experimental data is available for tungsten. The only stable lattice structure for W is the bcc structure, referred as α phase (type A2). Two other structures have been experimentally observed, the fcc and A15 structures, i.e., the γ (A1) and β (A15) phase, respectively. These states are metastable and convert back to the lowest energy phase at conversion temperatures >600 K for A15 and ≥ 700 K

TABLE I. Comparison of properties of tungsten bulk phases, different dimer configurations, and hydrogen solution in tungsten as obtained from experiment and DFT calculations: cohesive energy E_{coh} (eV/atom), lattice constant a (Å), atomic volume Ω (Å³), difference of cohesive energies with respect to E_{coh} of bcc phase ΔE_{coh} (eV/atom), binding energy E_b (eV/atom), dimer bond length r_0 (Å), enthalpy of solution S (eV), energy difference of octahedral (O) and tetrahedral (T) solution sites $\Delta E_{\text{O-T}}$ (eV), change in volume with H at T-site v_{H} (Å³ per H atom), migration energy E_m (eV), diffusion pre-exponential factor D_0 (m²/s), normal modes at the ground state, and saddle point ν , ν^{\ddagger} (THz). The imaginary frequency on the saddle point ν^* (THz) corresponds to vibration in the direction of the reaction coordinate.

	Expt.	DFT	
		Other	This work
bcc W			
E_{coh}	-8.89 ^a	-9.97 ^b , -7.41 ^c	-8.48
a	3.165 ^d	3.14 ^b , 3.22 ^c	3.172
Ω	15.87		15.96
fcc W			
ΔE_{coh}		0.50 ^e	0.49
a	4.13 ^a	3.960 ^e	4.025
A15 W			
ΔE_{coh}		0.08 ^f	0.09
a	5.05 ^a	5.06 ^f	5.059
H ₂ dimer			
E_b	-2.374 ^g		-2.267
r_0	0.741 ^g	0.75 ^h	0.751
WH dimer			
E_b		-1.374 ⁱ	-1.419
r_0	1.727 ^j	1.714 ⁱ	1.705
W ₂ dimer			
E_b	-2.5 ± 0.5 ^k	-2.05 ^c	-3.054
r_0	~2.2 ^k	1.95 ^c	1.860
H solution			
S	1.04 ± 0.17 ^l		0.95
$\Delta E_{\text{O-T}}$		0.38 ^m	0.38
v_{H}	2.9 ± 0.3 ⁿ		2.90
E_m	0.39 ± 0.09 ^l		0.21
D_0	4.1 ^{+5.0} _{-2.0} × 10 ⁻⁷ ^l		5.2 × 10 ⁻⁸
ν , ground state			46.7, 46.7, 34.7
ν^{\ddagger} , saddle point			63.3, 45.6
ν^*			i24.9

^aReference 1. E_{coh} derived from extrapolation of sublimation enthalpy to zero temperature.

^bReference 44, LDFT calculations.

^cReference 45, CASTEP code.

^dReferences 1 and 46–50.

^eReference 51.

^fReference 52, LDFT data normalized to experimental volume of bcc W.

^gReference 53.

^hReference 54, VASP code.

ⁱReference 45, GAUSSIAN 98 code.

^jReference 55.

^kReference 56.

^lReference 10. Experimental data 1100 K < T < 2500 K.

^mReferences 57 (CASTEP code) and 6 (VASP code).

ⁿAn averaged value for d -band metals given in Ref. 53.

for fcc structure.¹ In Table I, the calculated DFT results for existing bulk phases of W are presented. The calculated bcc lattice constant of 3.172 Å agrees well with the experimental value of 3.165 Å, and also the calculated lattice constants for the fcc and A15 structures are close to the experimental values. The differences in the calculated cohesive energies ΔE_{coh} for the fcc and A15 structures with respect to bcc

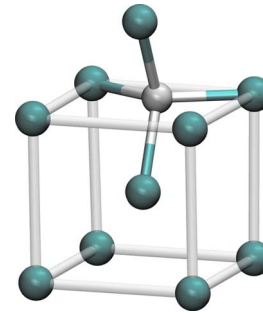


FIG. 1. (Color online) Hydrogen in its ground state at the tetrahedral interstitial site in bcc lattice bonding to its four nearest neighbors.

structure agree with the other DFT results in the literature. The W₂ dimer binding energy and bond length deviate somewhat from the experimental results, which is considered to be acceptable because of the relatively large uncertainty in the experimental values and because the main focus of this work is in the bulk properties. Using the semicore electron configuration $p^6d^5s^1$ instead of d^5s^1 provides W₂ binding energy and bond length of -2.35 eV/atom and 2.03 Å, respectively, which are closer to the experimental values. However, the bcc W lattice constant increases to 3.19 Å with $p^6d^5s^1$ configuration. Since a hydrogen atom at a solute site interacts with the outermost d and s electrons of the surrounding W atoms, whether the d^5s^1 or the semicore $p^6d^5s^1$ configuration for W atoms are used should have only a minor effect on the calculated hydrogen related properties. This was confirmed in the present calculations, there was no major change in the binding energy of WH dimer or the energies of H at different sites. Using the $p^6d^5s^1$ configuration yielded a 3% increase to the W–H dimer binding energy with r_0 unchanged and a 4% decrease in the H enthalpy of solution in the bulk.

B. H at solute site and diffusion in bcc W

Hydrogen has high diffusivity in bcc metals.⁵³ Ion-channeling experiments have shown that deuterium occupies the tetrahedral (T) site in single-crystal W,⁵⁸ which is also the result in our calculations, the T-site is energetically 0.38 eV lower than the octahedral (O) site. Figure 1 shows hydrogen in its ground state at the T-site. The hydrogen atom is bound to its four nearest neighbor W atoms, which share their electrons on the d and s orbitals with the s electron of H. The charge densities of H at T-site are presented in Fig. 2. The hydrogen enthalpy of solution S , i.e., the energy needed for an H atom to move from vacuum to a solute site in the bulk, was calculated with $S = E_{\text{H}}^{\text{sol}} - (E_0 + 1/2E_{\text{H}_2})$, where $E_{\text{H}}^{\text{sol}}$ is the total energy of H at a solute site, E_0 the reference energy of perfect bcc tungsten, and E_{H_2} the energy of the hydrogen dimer in vacuum. The resulted S agrees within the limits of accuracy with the experimental value given by Frauenfelder.¹⁰ The change in system volume, v_{H} , of H at T-site was calculated to be 2.90 Å³ per H atom. No experimental data for H volumes in W were found in the literature, although a whole range of v_{H} data in other metals is available. For bcc tantalum, with a slightly larger lattice constant

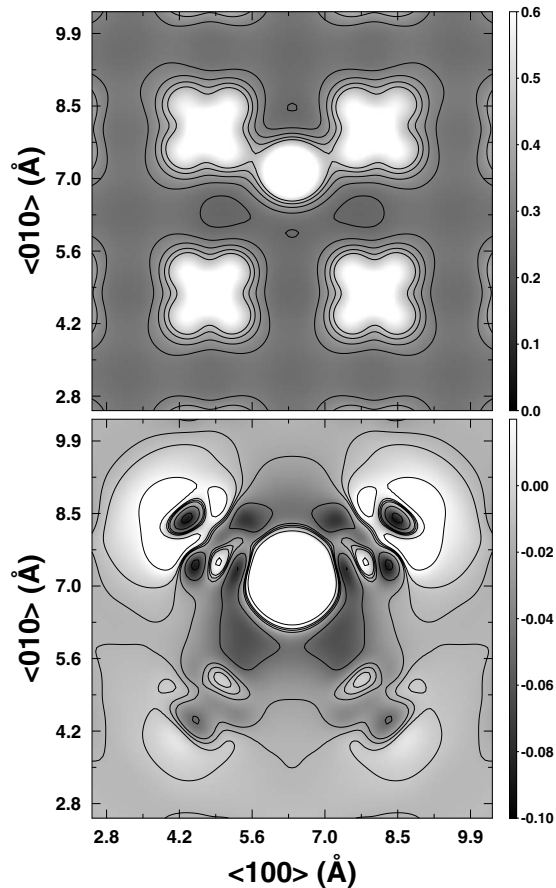


FIG. 2. Top: the charge densities for hydrogen located at a T-site in bcc W viewed on the (001) plane. Bonding to the nearest W atoms in-plane is apparent. Bottom: the difference in electron densities when inserting an H atom in T-site compared to pure W lattice. The lighter areas correspond to an increase and the darker areas to a decrease in the electron density.

($a_{Ta} \sim 3.31$ Å), the v_H has been experimentally found⁵⁹ to be 2.80 Å³. An average v_H for all d -band metals for T-site occupancy has been reported⁵³ (2.9 ± 0.3) Å³.

Hydrogen does not bond with other H atoms at nearby solute sites. This was concluded by locating two H atoms into adjacent T-sites ($\lambda = 1.12$ Å) and calculating the binding energy E_b^{H-H} as $E_b = (E_A + E_B) - (E_{AB} + E_0)$, where A and B refer to the H occupied neighboring T-sites. Positive E_b means attraction with this formulation. The H-H pair interaction was found to be strongly repulsive, $E_b^{H-H} = -1.139$ eV, which is consistent with the jellium model calculations⁴ and recent DFT calculations.^{5,6}

The height of the diffusion barrier for H migration was calculated using the NEB method as implemented in VASP. Two adjacent T-sites in the same plane were chosen as end points and seven intermediate images were used for interpolating the reaction path. The resulting barrier calculated with NEB is shown in Fig. 3. Taking into account the large energy difference $\Delta E_{O-T} = 0.38$ eV, we deduce that the reaction path of H always advances via neighboring T-sites in bcc W.

The quantum mechanical solution, Eq. (4), was used to calculate the hydrogen jump rate. The power of TST is the simple requirement of energies and vibrational frequencies at the ground state and transition state only, and can be applied when the tunneling effects are small. At lower temperatures,

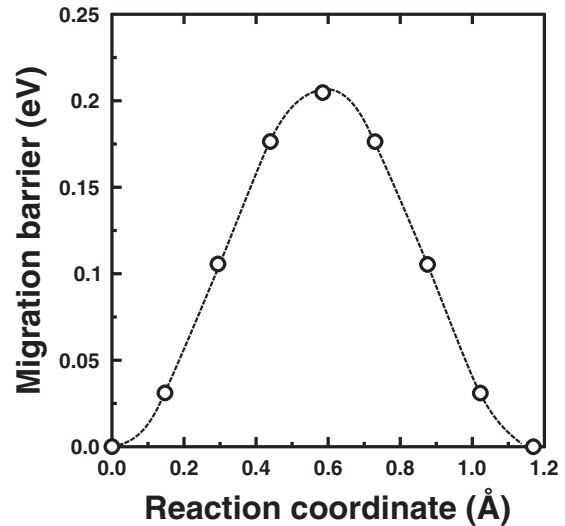


FIG. 3. Hydrogen migration barrier calculated with NEB. The dashed line is a barrier model by Wert and Zener (Ref. 30) $E(r) = 1/2 E_m \{1 - \cos(2\pi r/\Lambda)\}$, where r and Λ are the reaction coordinate and jump length of the diffusing particle along the reaction path, respectively.

tunneling effects become dominant and are discussed in Sec. III C. Due to the lightness of the H atom, the normal modes of its vibrational frequencies ν and ν^\ddagger , at the ground state and at the transition state, respectively, were calculated keeping the H atom decoupled from the surrounding W atoms, i.e., only H was allowed to vibrate. The results are presented in Table I. The effect of all-phonon calculations was $<1\%$ compared to the present calculations. The resulted three vibrational modes of H at the ground state ν have two degenerate frequencies and one smaller frequency. At the transition state there are two real normal modes of ν^\ddagger and one imaginary mode ν^* referring to the negative curvature of the saddle point in the direction of the reaction path.

The theoretical diffusion coefficient D has been calculated according to Eq. (1). The jump length was considered to be the distance of two adjacent T-sites from the DFT calculations ($\lambda = 1.12$ Å) and the jump rate was calculated from Eq. (4) ($\Gamma = \Gamma_{HTST}$). In Fig. 4 are presented the Arrhenius plots of the DFT results for D at temperatures from RT to 2500 K and the experimental D values from 850 to 2500 K. As was shown in Sec. II B, the TST provides a temperature dependent pre-exponential factor, i.e., $D_0 = D_0(T)$. Because the DFT calculated D in Fig. 4 show nearly linear Arrhenius behavior, a temperature independent pre-exponential factor was calculated to be $D_0 \cong D_0^{\text{eff}} = 5.2 \times 10^{-8}$ m²/s.

The experimental hydrogen diffusivities in W above RT by Frauenfelder,¹⁰ Zakharov *et al.*,¹¹ and Benamati *et al.*¹² are presented in Fig. 4. The effect of trapping in the experimental diffusivities is clearly seen in the data points at temperatures below 1100 K, where the values by Zakharov and Benamati fall under the extrapolated D from the high temperature region by Frauenfelder. In addition, in the work of Benamati the W samples were doped with 5% of rhenium, which can act as an additional trapping site.

Serra *et al.*¹⁴ and Benamati *et al.*¹² suggest that the differences in H diffusivities and solubilities measured by Frauenfelder¹⁰ and Zakharov *et al.*,¹¹ could be explained if it

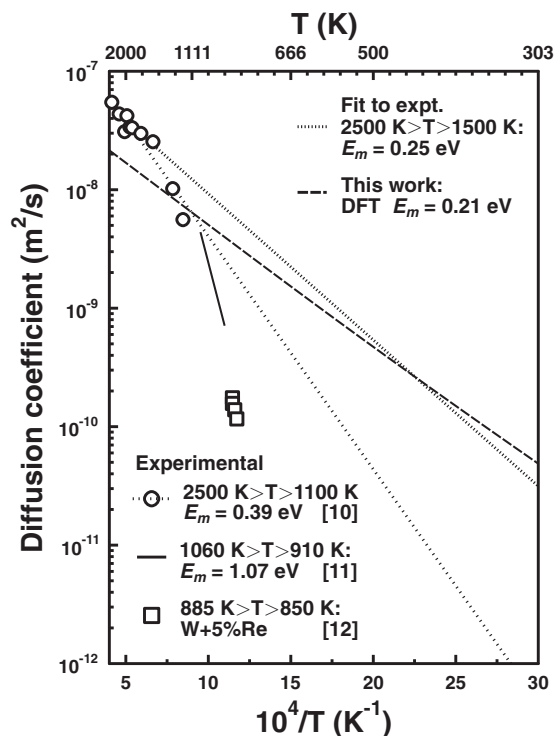


FIG. 4. Calculated hydrogen diffusion coefficient D compared to the experimental values. The trapping effect gets pronounced at temperatures below 1100 K, where the experimental D values fall under the extrapolated Arrhenius fit of the Frauenfelder data (Ref. 10) (dotted line with wide spacing). Omitting the two lowest experimental points in Frauenfelder data, decreases the migration barrier from 0.39 to 0.25 eV.

is assumed that hydrogen diffusion is strongly influenced by trapping effects even up to temperatures of about 1500 K. Following this conclusion, in a numerical fit to Frauenfelder's data only the data points obtained at temperatures above 1500 K were kept. The fitted H pre-exponential factor and migration energy to the given temperature region were found to be $D_0 = 1.58 \times 10^{-7} \text{ m}^2/\text{s}$ and $E_m = 0.25 \text{ eV}$, respectively. These fitted values are in good agreement with the values calculated using DFT ($D_0^{\text{eff}} = 5.2 \times 10^{-8} \text{ m}^2/\text{s}$, $E_m = 0.21 \text{ eV}$). The assumption by Serra and Benamati leading to exclusion of only two points from the Frauenfelder data, has made an $\sim 61\%$ and $\sim 36\%$ decrease to the D_0 and E_m values, respectively. Another fact in favor of omitting the two lowest data points, is that the original Frauenfelder pre-exponential factor $D_0 = 4.1 \times 10^{-7} \text{ m}^2/\text{s}$ gives an unrealistic high H jump frequency of $\sim 200 \text{ THz}$ when using Eq. (1). Noteworthy is also to mention that in Frauenfelder's work, the frequency was calculated using the Wert and Zener³⁰ model $\nu_0 = (E_m/2m\lambda^2)^{1/2}$ with jump length λ corresponding to jumps between neighboring O-sites. Using the same model with λ for T-site jumps and $E_m = 0.25 \text{ eV}$, we obtain $\nu_0 = 30 \text{ THz}$, which is close to our calculated value $\nu_0 = 26 \text{ THz}$ obtained for the classical regime with Eq. (3). It is also interesting to note that in hydrogen diffusivity studies in Ta, which has only one d electron less than W, the resulting H diffusion coefficient $4.2 \times 10^{-8} \exp(-0.136 \text{ eV}/kT) \text{ m}^2/\text{s}$ is very similar to the results calculated in this work.⁶⁰

Another point of view to the discussion of the discrepancies in the theoretical and experimental results is the DFT related limitation of obtaining correct heights of diffusion barriers. It has been shown that calculations with ordinary generalized gradient approximation (GGA) functionals can give deviating barrier heights compared with calculations with more sophisticated quantum chemistry techniques, e.g., the Hartree–Fock method.⁶¹ Moreover, the use of GGA functional provide 0.05 eV lower migration energy compared with experimental result for hydrogen studies in bulk fcc Ni.⁶² The revised PBE (rPBE) functionals have been shown to enhance the hydrogen adsorption energies on surfaces⁶³ and the configuration interaction calculations can provide more accurate ground states for the transition metals. Still, we think that the DFT related issues cannot solely explain the discrepancy between the theoretical and experimental hydrogen diffusivity in tungsten.

C. Effect of tunneling

At very low temperatures, the effect of tunneling plays an important role in deducing the H hopping rate. Macrander *et al.*¹⁵ studied H diffusion in W at 29 K using field-ion microscopy method. In their work it was concluded, that the diffusion of H in tungsten should be treated as a nonclassical event. Their diffusion coefficient $D(29 \text{ K}) = (1-10) \times 10^{-22} \text{ m}^2/\text{s}$ is clearly higher than the classical diffusion coefficient $D(29 \text{ K}) = 6.9 \times 10^{-75} \text{ m}^2/\text{s}$ extrapolated from the Frauenfelder's results.

The theory of tunneling has been studied for decades.⁶⁴ In this work, the tunneling effect has been studied using two simple models, which are founded on introducing a tunneling correction factor to Γ_{HTST} . In hTST tunneling there is no coupling between the diffusing hydrogen and the surrounding lattice phonons or the conduction electrons. In more sophisticated tunneling methods, this adiabaticity is eliminated and the diffusing ion is coupled to the phonons or to the conduction electrons of the host lattice. The small polaron theory^{65,66} and further the phonon assisted tunneling theory⁶⁷ have been developed for the diffusion of light interstitial atoms in metals at low temperatures. The model for nonadiabatic coupling of the hydrogen movement to the conducting electrons have been presented for low temperatures, where the phonon assisted tunneling becomes eliminated.^{68,69} Examples of DFT calculations on hydrogen tunneling combining phonon coupling⁷⁰ and conduction electron coupling⁴³ over wide range of temperature can be found in the literature.

Commonly the barrier for tunneling is thought as an infinite, one-dimensional parabola with an imaginary frequency on the saddle point. Wigner,³⁶ and Hirschfelder and Wigner⁷¹ presented a harmonic correction factor $x^*/\sin x^*$, which yields for the jump rate

$$\Gamma_{\text{HTST}}^{\text{Wig}} = \frac{x^*}{\sin x^*} \times \Gamma_{\text{HTST}} \quad (6)$$

Γ_{HTST} is the jump rate as in Eq. (4) and $x^* = \hbar|\nu^*|/2kT$, where ν^* is the imaginary frequency at the saddle point. In Fig. 5, the Wigner corrected jump rate for H is illustrated. The effect of tunneling increases at lower temperatures and becomes a

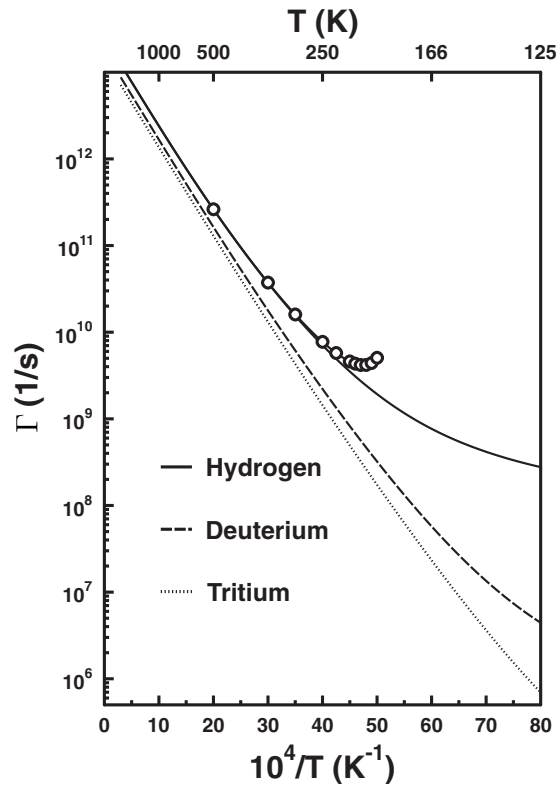


FIG. 5. Theoretical jump rates for hydrogen isotopes with tunneling correction for the truncated parabolic barrier taken into account as in the SCTST model by Ferrmann and Auerbach (Ref. 72). The open circles (○) represent the harmonic result for hydrogen Γ as calculated by the Wigner tunneling model (Ref. 36).

dominant effect compared to harmonic TST under a certain tunneling crossover temperature. In Wigner's model the crossover temperature is $T_c = h|v^*|/(2\pi k) \approx 190$ K for H in tungsten. The Wigner model is not continuous since Eq. (6) diverges to infinity when $T \rightarrow T_c$, which is clearly seen in Fig. 5.

Ferrmann and Auerbach⁷² developed a separable semiclassical TST (SCTST) for a truncated parabolic barrier with the imaginary frequency at the saddle point. In their SCTST the jump rate is continuous in the whole temperature range. The tunneling correction Γ_{corr} for this barrier is

$$\Gamma_{\text{corr}}(T) = \frac{e^{\beta \Delta E_m^{\text{ZPE}}}}{1 + e^{2\theta_0}} + \frac{1}{2} \int_{-\infty}^{\theta_0} e^{\beta h v^* \theta / \pi} \sec^2 \theta d\theta, \quad (7)$$

where $\Delta E_m^{\text{ZPE}} = E_m + \Delta E_{\text{ZPE}}$, $\beta = 1/(kT)$, and the maximum barrier penetration integral $\theta_0 = \pi \Delta E_m^{\text{ZPE}} / (h|v^*|)$. Equation (7) has been solved numerically and the tunneling corrected jump rate over the whole T range is now

$$\Gamma_{\text{SCTST}} = \Gamma_{\text{HTST}} \times \Gamma_{\text{corr}}, \quad (8)$$

where Γ_{HTST} is given by Eq. (4). The tunneling crossover temperature in SCTST is

$$T_c = \frac{h|v^*| \Delta E_m^{\text{ZPE}} / k}{2\pi \Delta E_m^{\text{ZPE}} - h|v^*| \ln 2}. \quad (9)$$

For H frequencies given in Table I, Eq. (9) yields $T_c \approx 204$ K. In Fig. 5 are presented the jump rates for H, D, and T calculated with SCTST. At low temperatures ($T < T_c$),

D and T are nearly immobile compared to the H. At higher temperatures ($T > T_c$) the tunneling effect vanishes and the isotope effect becomes classically $1/\sqrt{m}$ dependent.

A more refined SCTST approximation is the nonseparable, anharmonic SCTST developed in the work by Peters *et al.*⁷³ In their work, with proton exchange calculations for $\text{NH}_2 + \text{CH}_4$ molecules, it was concluded that Γ_{corr} by Ferrmann and Auerbach overestimates the jump rate since their truncated barrier model omits part of the potential barrier profile. This can be also concluded in our calculations since the diffusion coefficient calculated with Eq. (8) is $6.3 \times 10^{-14} \text{ m}^2/\text{s}$ at 29 K. Our result overestimates the tunneling diffusion constant as expected but gives an apparent indication of the importance of tunneling since the DFT result is much closer to the experimental $D(29 \text{ K})$ than the extrapolated result by Frauenfelder.

IV. SUMMARY AND CONCLUSIONS

Hydrogen diffusion in bcc tungsten has been studied using DFT calculations. The diffusion barrier between two adjacent ground states was calculated with the NEB method and the diffusion coefficient was deduced with vibrational mode calculations according to the TST. The temperature range in the calculations was from RT to 2500 K. The resulting diffusion parameters showed fairly good compliance with the high temperature experimental data above 1500 K. As suggested by Serra *et al.*¹⁴ and Benamati *et al.*¹² this leads to the conclusion that trapping can play an important role at temperatures below 1500 K. Also the DFT related errors has to be considered. However, the authors think that these cannot exclusively explain the differences between the theoretical and experimental H diffusion results.

The tunneling effect has been discussed using two simple tunneling models. Both of these models result in nearly the same crossover temperature ~ 200 K, under which the nonclassical barrier penetration becomes significant. The truncated barrier model by Ferrmann and Auerbach⁷² provides an overestimated D at 29 K compared to the experimental result but is by far more consistent than the extrapolated experimental result by Frauenfelder.¹⁰ The influence of tunneling to the isotope effect has been studied experimentally at 80 K.¹⁶ Our calculations are in agreement with these results, as per H is mobile even at low temperatures whereas the mobility of deuterium and tritium is several orders of magnitude smaller.

ACKNOWLEDGMENTS

This work, supported by the European Communities under the contract of Association between Euratom-Tekes, was carried out within the framework of the European Fusion Development Agreement (EFDA). The views and opinions expressed herein do not necessarily reflect those of the European Commission. Grants of computer time from the Center for Scientific Computing (CSC) in Espoo, Finland are gratefully acknowledged.

¹E. Lassner and W.-D. Schubert, *Tungsten: Properties, Chemistry, Technology of the Element, Alloys, and Chemical Compounds* (Kluwer Academic, New York, 1999).

- ²A. Loarte, B. Lipschultz, A. Kukushkin, G. Matthews, P. Stangeby, N. Asakura, G. Counsell, G. Federici, A. Kallenbach, K. Krieger, A. Mahdavi, V. Philipps, D. Reiter, J. Roth, J. Strachan, D. Whyte, R. Doerner, T. Eich, W. Fundamenski, A. Herrmann, M. Fenstermacher, P. Ghendrih, M. Groth, A. Kirschner, S. Konoshima, B. LaBombard, P. Lang, A.W. Leonard, P. Monier-Garbet, R. Neu, H. Pacher, B. Pegourie, R.A. Pitts, S. Takamura, J. Terry, and E. Tsitrone, *Nucl. Fusion* **47**, S203 (2007).
- ³C. S. Becquart and C. Domain, *Phys. Rev. Lett.* **97**, 196402 (2006).
- ⁴J. K. Nørskov, *Phys. Rev. B* **20**, 446 (1979).
- ⁵K. O. E. Henriksson, K. Nordlund, A. Krashennnikov, and J. Keinonen, *Appl. Phys. Lett.* **87**, 163113 (2005).
- ⁶C. Becquart and C. Domain, *J. Nucl. Mater.* **386–388**, 109 (2009).
- ⁷W. Wang, J. Roth, S. Lindig, and C. H. Wu, *J. Nucl. Mater.* **299**, 124 (2001).
- ⁸G. E. Moore and F. C. Unterwald, *J. Chem. Phys.* **40**, 2639 (1964).
- ⁹L. N. Ryabchikov, *Ukr. Fiz. Zh.* **9**, 293 (1964).
- ¹⁰R. Frauenfelder, *J. Vac. Sci. Technol.* **6**, 388 (1969).
- ¹¹A. P. Zakharov, V. M. Sharapov, and E. I. Evko, *Fiz.-Khim. Mekh.* **9**, 29 (1973).
- ¹²G. Benamati, E. Serra, and C. H. Wu, *J. Nucl. Mater.* **283–287**, 1033 (2000).
- ¹³R. A. Causey and T. J. Venhaus, *Phys. Scr.* **T94**, 9 (2001).
- ¹⁴E. Serra, G. Benamati, and O. V. Ogorodnikova, *J. Nucl. Mater.* **255**, 105 (1998).
- ¹⁵A. T. Macrander and D. N. Seidman, *J. Appl. Phys.* **56**, 1623 (1984).
- ¹⁶J. A. Panitz, *J. Vac. Sci. Technol.* **14**, 502 (1977).
- ¹⁷F. Maury, M. Biget, P. Vajda, A. Lucasson, and P. Lucasson, *Radiat. Eff. Defects Solids* **38**, 53 (1978).
- ¹⁸G. Kresse and J. Hafner, *Phys. Rev. B* **47**, 558 (1993).
- ¹⁹G. Kresse and J. Hafner, *Phys. Rev. B* **49**, 14251 (1994).
- ²⁰G. Kresse and J. Furthmüller, *Phys. Rev. B* **54**, 11169 (1996).
- ²¹P. E. Blöchl, *Phys. Rev. B* **50**, 17953 (1994).
- ²²G. Kresse and D. Joubert, *Phys. Rev. B* **59**, 1758 (1999).
- ²³J. P. Perdew, K. Burke, and M. Ernzerhof, *Phys. Rev. Lett.* **77**, 3865 (1996).
- ²⁴Y. Zhang and W. Yang, *Phys. Rev. Lett.* **80**, 890 (1998).
- ²⁵M. Methfessel and A. T. Paxton, *Phys. Rev. B* **40**, 3616 (1989).
- ²⁶W. H. Press, B. P. Flannery, and S. A. Teukolsky, *Numerical Recipes: The Art of Scientific Computing* (Cambridge University Press, Cambridge, 1986).
- ²⁷H. J. Monkhorst and J. D. Pack, *Phys. Rev. B* **13**, 5188 (1976).
- ²⁸G. Mills, H. Jonsson, and G. K. Schenter, *Surf. Sci.* **324**, 305 (1995).
- ²⁹H. Jonsson, G. Mills, and K. W. Jacobsen, *Classical and Quantum Dynamics in Condensed Phase Simulations* (World Scientific, New Jersey/London, 1998).
- ³⁰C. Wert and C. Zener, *Phys. Rev.* **76**, 1169 (1949).
- ³¹C. Wert, *Phys. Rev.* **79**, 601 (1950).
- ³²C. Zener, *Imperfections in Nearly Perfect Crystals* (Wiley, New York, 1952).
- ³³J. Philibert, *Atom Movements: Diffusion and Mass Transport in Solids* (Les Éditions de Physique, France, 1991).
- ³⁴H. Eyring, *J. Chem. Phys.* **3**, 107 (1935).
- ³⁵H. Eyring, *Trans. Faraday Soc.* **34**, 41 (1938).
- ³⁶E. Wigner, *Z. Phys. Chem. Abt. B* **19**, 203 (1932).
- ³⁷E. Wigner, *Trans. Faraday Soc.* **34**, 29 (1938).
- ³⁸G. H. Vineyard, *J. Phys. Chem. Solids* **3**, 121 (1957).
- ³⁹N. Sandberg, B. Magyar-Köpe, and T. R. Mattsson, *Phys. Rev. Lett.* **89**, 065901 (2002).
- ⁴⁰M. Mantina, Y. Wang, R. Arroyave, L. Q. Chen, Z. K. Liu, and C. Wolverton, *Phys. Rev. Lett.* **100**, 215901 (2008).
- ⁴¹P. G. Sundell and G. Wahnström, *Phys. Rev. B* **70**, 224301 (2004).
- ⁴²D. E. Jiang and E. A. Carter, *Phys. Rev. B* **70**, 064102 (2004).
- ⁴³P. G. Sundell and G. Wahnström, *Phys. Rev. B* **70**, 081403 (2004).
- ⁴⁴T. Ochs, O. Beck, C. Elsasser, and B. Meyer, *Philos. Mag. A* **80**, 351 (2000).
- ⁴⁵N. Juslin, P. Erhart, P. Träskelin, J. Nord, K. O. E. Henriksson, K. Nordlund, E. Salonen, and K. Albe, *J. Appl. Phys.* **98**, 123520 (2005).
- ⁴⁶*International Tables for Crystallography*, edited by A. J. C. Wilson (Kluwer Academic, Dordrecht, Boston, London, 1995), Vol. C.
- ⁴⁷*CRC Handbook of Chemistry and Physics*, 85th ed., edited by D. R. Lide (CRC, Boca Raton, 2004).
- ⁴⁸A. G. Every and A. K. McCurdy, *Landolt-Börnstein New Series: Numerical Data and Functional Relationships in Science and Technology* (Springer, Berlin, 1992).
- ⁴⁹D. I. Bolef and J. D. Klerk, *J. Appl. Phys.* **33**, 2311 (1962).
- ⁵⁰J. H. Rose, J. R. Smith, F. Guinea, and J. Ferrante, *Phys. Rev. B* **29**, 2963 (1984).
- ⁵¹K. Einarsdotter, B. Sadigh, G. Grimvall, and V. Ozolinš, *Phys. Rev. Lett.* **79**, 2073 (1997).
- ⁵²M. Mrovec, R. Gröger, A. G. Bailey, D. Nguyen-Manh, C. Elsässer, and V. Vitek, *Phys. Rev. B* **75**, 104119 (2007).
- ⁵³Y. Fukai, *The Metal-Hydrogen System*, 2nd ed. (Springer, Berlin, 2005).
- ⁵⁴G. Kresse, *Phys. Rev. B* **62**, 8295 (2000).
- ⁵⁵X. Wang and L. Andrews, *J. Phys. Chem. A* **106**, 6720 (2002).
- ⁵⁶M. D. Morse, *Chem. Rev.* **86**, 1049 (1986).
- ⁵⁷K. O. E. Henriksson, K. Nordlund, A. Krashennnikov, and J. Keinonen, *Fusion Sci. Technol.* **50**, 43 (2006).
- ⁵⁸S. T. Picraux and F. L. Vook, *Phys. Rev. Lett.* **33**, 1216 (1974).
- ⁵⁹H. Peisl, *Topics in Applied Physics*, Hydrogen in Metals I (Springer, Berlin, Heidelberg, 1978), Vol. 28.
- ⁶⁰Z. Qi, J. Volkl, R. Lasser, and H. Wenzl, *J. Phys. F: Met. Phys.* **13**, 2053 (1983).
- ⁶¹V. Barone and C. Adamo, *J. Chem. Phys.* **105**, 11007 (1996).
- ⁶²E. Wimmer, W. Wolf, J. Sticht, P. Saxe, C. B. Geller, R. Najafabadi, and G. A. Young, *Phys. Rev. B* **77**, 134305 (2008).
- ⁶³B. Hammer, L. B. Hansen, and J. K. Nørskov, *Phys. Rev. B* **59**, 7413 (1999).
- ⁶⁴H. Grabert and H. R. Schober, *Topics in Applied Physics*, Hydrogen in Metals III (Springer, Berlin, Heidelberg, 1997), Vol. 73.
- ⁶⁵J. Yamashita and T. Kurosawa, *J. Phys. Chem. Solids* **5**, 34 (1958).
- ⁶⁶T. Holstein, *Ann. Phys.* **8**, 343 (1959).
- ⁶⁷C. P. Flynn and A. M. Stoneham, *Phys. Rev. B* **1**, 3966 (1970).
- ⁶⁸J. Kondo, *Physica B* **125**, 279 (1984).
- ⁶⁹J. Kondo, *Physica B* **126**, 377 (1984).
- ⁷⁰P. G. Sundell, M. E. Björketun, and G. Wahnström, *Phys. Rev. B* **76**, 094301 (2007).
- ⁷¹J. O. Hirschfelder and E. Wigner, *J. Chem. Phys.* **7**, 616 (1939).
- ⁷²J. T. Fermann and S. Auerbach, *J. Chem. Phys.* **112**, 6787 (2000).
- ⁷³B. Peters, A. T. Bell, and A. Chakraborty, *J. Chem. Phys.* **121**, 4461 (2004).